Results in Physics 14 (2019) 102423

Contents lists available at ScienceDirect

Results in Physics

journal homepage: www.elsevier.com/locate/rinp

Corrosion resistance and morphological deterioration of 316Ti austenitic, GX4CrNiMo16-5-1 martensitic and 444 ferritic stainless steels in aqueous corrosive environments

Roland Tolulope Loto

Department of Mechanical Engineering, Covenant University, Ota, Ogun State, Nigeria

ARTICLE INFO

Keywords:
Corrosion
Steel
Pitting
Passivation

ABSTRACT

The corrosion resistance of 316Ti austenitic, GX4CrNiMo16-5-1 martensitic and 444 ferritic stainless steels in 1 M H_2SO_4 solution at 0%–6% NaCl concentration was studied by potentiodynamic polarization, open circuit potential measurement and optical microscopy characterization. GX4CrNiMo16-5-1 exhibited the lowest corrosion rate result with optimal value of 4.073 mm/y compared to 316Ti and 444 steels with optimal values of 16.033 mm/y and 20.844 mm/y. The corrosion rate of GX4CrNiMo16-5-1 decreased with increase in NaCl concentration. GX4CrNiMo16-5-1 exhibited the highest pitting resistance at all NaCl concentrations, sustaining its passive film throughout compared to 316Ti and 444 steels whose passivity were lost at 1% and 2% NaCl concentrations. The OCP plots of GX4CrNiMo16-5-1 where significantly electropositive with significant positive displacement compared to 316Ti and 444 steel whose OCP values were electronegative. Optical morphological characterization of the steels shows the absence of localized corrosion deterioration on 316Ti though the steel generally corroded. 444 steel exhibited significant pitting corrosion compared to GX4CrNiMo16-5-1 with visible intergranular corrosion.

Introduction

Stainless steels are ferrous alloys composed of minimum 10.5% Cr content and are exceptionally useful as structural parts in industrial applications due to their excellent mechanical and corrosion resistant properties [1,2]. Cr enables the formation of a protective passive film on stainless steels, while the presence of Ni stabilizes the film [3]. Currently there are numerous stainless steel types commercially available however, inappropriate selection of the steel alloys for application in specific industrial environments is one of the major causes of corrosion and accelerated deterioration of the steels. Corrosion of stainless steel alloys and equipment in aqueous industrial environments containing SO_4^{2-} and Cl^- anions has been one of the most important problems in chemical processing, petroleum refining, energy generation, fertilizer production, marine and desalination plants. Other very important determinant factors responsible for stainless steel corrosion includes microstructural inhomogeneities on the steel surface, specific alloy additions (Ti, N, B etc.), concentration of anions in the environment (SO_4^{2-}, Cl^-, O_2 etc.) and amount (wt%) of corrosion resisting elements e.g. Cr, Ni within the steels [4–9].

Industrial application of some stainless steels is uneconomical and costly for the environment to which they are applied [10]. Documentation of the corrosion resistance of stainless steels to variation in concentration of Cl^- and SO_4^{2-} anions in corrosive environments for appropriate material selection and sustainability of industrial parts and structures during service is of utmost importance. Their corrosion resistance is a function of the resilience and stability of their passive film which prevents the onset of localized corrosion reactions such as pitting corrosion [11]. Pitting corrosion is prevalent in stainless steels, and the localized corrosion resistance of stainless steels depends on (i) concentration of corrosive anions within the environment and (ii) the ability of their protective films to withstand the adsorption of corrosive anions such as chlorides and sulphates [12].

Research on stainless steels has shown that they have their unique response to the onset and propagation of localized corrosion reactions in corrosive environments. This varies with the type of steel and the degree of corrosivity of the environment as earlier stated [13–18]. The research within this manuscript focuses on the corrosion resistance and onset of pitting corrosion of 316Ti austenitic, GX4CrNiMo16-5-1 martensitic and 444 ferritic stainless steel in sulphate environment at various chloride concentrations. 316Ti austenitic stainless steel is a titanium stabilised 316 steel with applications in chemical processing, marine, oil and gas, automotive, steam boilers, hot water tanks, and processing and reaction vessels.

E-mail address: tolu.loto@gmail.com.

https://doi.org/10.1016/j.rinp.2019.102423
Received 13 May 2019; Received in revised form 3 June 2019; Accepted 5 June 2019
Available online 08 June 2019

Intergranular corrosion behaviour of 316Ti austenitic stainless steels was studied with respect variation of Ti, C and N concentrations. Results showed Ti increase the intergranular corrosion resistance of the steel [19]. Decrease in C contents increases sensitization resistance steel while Mo was determined to decrease the precipitation of Cr-rich carbides [20]. The work of Zatkalíková et al [21], shows polished surface finishing of 316Ti in 5% $FeCl_3$ has no effect on its pitting corrosion resistance. GX4CrNiMo16-5-1 martensitic stainless steel is formulated for casting and is suitable for areas with risk of corrosion in water and steam. It is also used in the manufacture of pumps, turbine parts, fittings, compressor components in power stations, machine construction, and chemical industry. 444 ferritic stainless steel is a low carbon, dual stabilised, molybdenum containing steel with good ductility, toughness and resistance to sensitisation. It is used in food processing, hot-water tanks, heat exchanger tubing and automotive components. The steel exhibited sufficient resistance to pitting corrosion in phosphate buffer solution for application as dental implants [22]. Investigation of the pitting resistance of 444 ferritic steel for application as drinking water tanks walls shows it proffers no additional advantage compared to the conventional 304 austenitic steel [23]. Research by Part and Lee [24], showed that chloride ions destroys the crevice corrosion resistance of AISI 444. The corrosion behaviour of the three stainless steels to be studied, the response of their protective oxide to chloride concentration and breakdown of the film is key to achieving the primary objective of this research.

Experimental methods

316Ti austenitic stainless steel (316Ti), GX4CrNiMo16-5 cast martensitic stainless steel (GX4Cr) and 444 ferritic stainless steel (444St) sheets from Vienna University of Technology, Vienna, Austria were analysed with PhenomWorld scanning electron microscope (Model No. MVE0224651193) at the Materials Characterization Laboratory in Department of Mechanical Engineering, Covenant University, Ota, Ogun State, Nigeria to obtain their elemental composition (wt%) is shown in Table 1. The steels were cut to dimensions with surface areas of 1 cm^2 and thereafter embedded in Versocit acrylic resin mounts. The exposed area of the steels were metallographically prepared starting with the use of emery abrasive papers (120, 240, 320, 600, 800 and 1000 grits) to grind and polish the steels before using 6 µm diamond polishing paste and thereafter cleansed with distilled H_2O and acetone. 200 ml of 1 M H_2SO_4 solution at 0%, 1%, 2%, 3%, 4%, 5% and 6% NaCl volumetric concentration were prepared from analar grade reagent of the acid and NaCl.

Potentiodynamic polarization test and open circuit potential measurement was performed on (316Ti), (GX4Cr) and (444St) stainless steels by potentiodynamic polarization and open circuit potential measurement at ambient temperature of 30 °C using a three electrode connecting system (acrylic mounted steel electrodes, Accumet Ag/AgCl reference electrode and platinum counter electrode). The electrodes were submerged in 200 ml of the acid-chloride test electrolyte within a transparent glass cell, and interfaced with Digi-Ivy 2311 potentiostat and computer. Plotted polarization curve were produced at scan rate of 0.0015 V s^{-1} between potentials of −1.5 V and +1.5 V. Corrosion current density, C_D (A/cm^2) and corrosion potential, C_P (V) were determined from the plots by Tafel extrapolation method.

Table 1
Composition (wt%) of 316Ti, GX4Cr and 444St.

316Ti													
Element	C	Si	Mn	P	S	Cr	Mo	Ni	Ti	N	Cu	V	Fe
Content	0.08	0.8	2	0.05	0	18	3	14	0.7	0.1	0	0	61.3
GX4Cr													
Element	C	Si	Mn	P	S	Cr	Mo	Ni	Ti	N	Cu	V	Fe
Content	0.06	0.8	1	0.04	0	17	1.5	6	0	0	0.3	0.1	73.21
444St													
Element	C	Si	Mn	P	S	Cr	Mo	Ni	Ti	N	Cu	V	Fe
Content	0.03	1	1	0.04	0	19	2	1	0.2	0.04	0	0	77.48

Corrosion rate C_R (mm/y) was determined as follows [25];

$$C_R = \frac{0.00327 \times C_D \times E_{QV}}{D} \quad (1)$$

E_{QV} is the equivalent weight (g) of stainless steel, 0.003 27 is a corrosion rate constant and D is the density (g) of the steel. Polarization resistance, R_p, (Ω) was calculated from Eq. (2) below [26,27];

$$R_p = 2.303 \frac{B_a B_c}{B_a + B_c}\left(\frac{1}{I_{cr}}\right) \quad (2)$$

where B_a is the anodic Tafel slope and B_c is the cathodic Tafel slope, both are measured as (V/dec). Open circuit potential measurements was performed (with Digi-ivy potentiostat) at step potential of 0.2 V s^{-1} for 5400 s in 1 M H_2SO_4 at 0%, 1% and 6% NaCl concentration with Ag/AgCl reference electrode and acrylic mounted steel working electrode. Optical images of the stainless steel specimens before and after corrosion test from 1 M H_2SO_4 solution at 0%, 1% and 6% NaCl concentration were captured and analysed with Omax trinocular metallurgical microscope.

Results and discussion

Potentiodynamic polarization studies

Potentiodynamic polarization plots of 316Ti, GX4Cr and 444St corrosion in 1 M H_2SO_4 solution at 0%, 1%, 2%, 3%, 4%, 5% and 6% NaCl concentration are shown from Figs. 1–3. Table 2 shows the corrosion rate, corrosion current density, corrosion potential, polarization resistance and Tafel slopes data from the polarization plots. The corrosion rate data (Table 2) shows GX4Cr steel was significantly more corrosion resistant than 316Ti and 444St in the acid chloride solution. At 0% NaCl, GX4Cr had a corrosion rate value of 0.373 mm/y corresponding to corrosion current density of 3.48×10^5 A/cm^2. This is significantly lower than the values of 8.022 mm/y and 15.945 mm/y for 316Ti and 444St at the same NaCl concentration. Increase in NaCl concentration caused a relative increase in corrosion rate value which peaked at 2% NaCl (4.328 mm/y), further increase in NaCl concentration results in significant decrease in corrosion rate value of GX4Cr steel to 1.066 mm/y at 9.92×10^5 A/cm^2 (6% NaCl). Observation of the corrosion potential value of GX4Cr steel shows significant cathodic shift from −0.243 V (0% NaCl) to −0.316 V at 1% NaCl. The corrosion potential value continued to shift cathodically with increase in NaCl concentration indicating (i) dominant H_2 evolution and O_2 reduction reactions, and (ii) localized deterioration of the steel due to the electrochemical action of increased Cl^- ions. The corrosion rate value shows decrease in general corrosion after 2% NaCl; however, the corrosion potential becomes more electronegative with respect to NaCl concentration. This shows two contrasting phenomena which is prevalent in passivating alloys. Decrease in general corrosion does not necessarily connote localized corrosion resistance as shown in the corrosion potential values. The competitive adsorption of $SO4^{2-}$ and excess Cl^- ions might have played a major role in the decline in value; nevertheless Cl^- ions would have diffused through the passive film to initiate localized corrosion reactions.

Increase in NaCl concentration beyond 1% did not have significant influence on the corrosion resistance of 316Ti till 5% and 6% NaCl where the increase in corrosion rate was minimal. However, the increase in corrosion potential after 0% NaCl concentration to relative electropositive values (−0.419 V to −0.409 V) shows oxidation reactions dominated the corrosion reaction processes, though the anodic-cathodic Tafel slope values redox electrochemical processes counterbalanced each other. Oxidation reaction mechanisms are directly related to general surface deterioration, but yet signifying strong

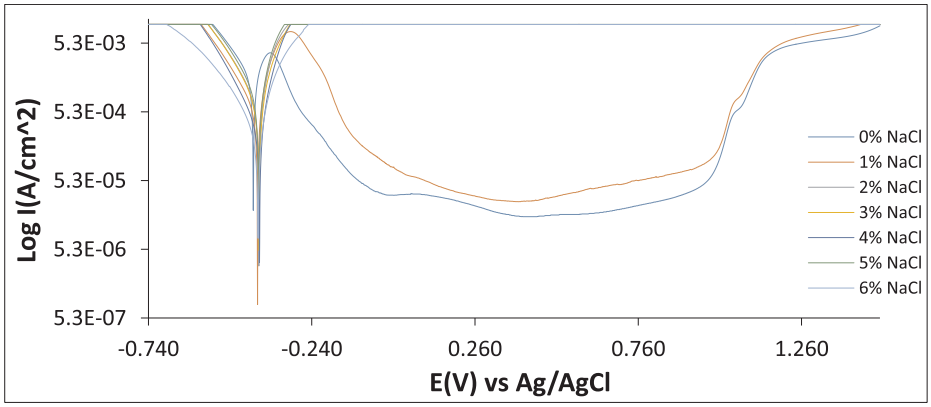

Fig. 1. Potentiodynamic polarization plots 316Ti corrosion in 1 M H_2SO_4 solution at 0% − 6% NaCl concentration.

resistance to localized corrosion. Further increase in NaCl concentration beyond 1% shifted the corrosion potential further causing slight increase in oxidation reactions till 5% NaCl where there was minimal change in corrosion potential to electronegative values. The assertion of vulnerability of 316Ti to general surface deterioration compared to GX4Cr is further confirmed from comparison of their polarization resistance values. The lower polarization resistance values of 316Ti shows it is more polarized than GX4Cr hence oxidizes at relatively faster rate than GX4Cr. The corrosion rate of 444St coupled with its polarization resistance values is comparable to 316Ti (excluding 0% and 6% NaCl). Its corrosion potential values indicate general and limited localized corrosion reaction mechanisms.

Potentiostatic studies

Pitting corrosion is prevalent on passivating steels in solutions containing SO_4^{2-} and Cl^- ions. Potentiostatic data (metastable pitting, pitting potential and passivation range) from polarization test for 316Ti, GX4Cr and 444St stainless steels are shown in Table 3. Fig. 4(a) and (b) shows the metastable pitting and stable pitting portion of the polarization plots of 316Ti while Figs. 5(a) and 6(b) shows the metastable pitting and stable pitting portion of GX4Cr and 444St steels. GX4Cr exhibited the highest pitting resistance at all NaCl concentrations (0% − 6% NaCl) in the acid solutions. At 0% NaCl, the pitting potential of GX4Cr plot in Fig. 5(b) is 0.914 V corresponding to pitting current value of 2.13×10^5 A. Increase in NaCl concentration caused a corresponding increase in pitting potential value as shown in the plots [Fig. 5(b)] till 3% NaCl signifying enhanced resistance to pitting corrosion. This observation is due to the adsorption of Cl^- ions resulting in the formation of chloride complexes at the steel solution interface; hence it gives the steel pseudo resistance to localized corrosion before breakdown at the transpassive region of the polarization plots. Further increase in NaCl concentration beyond 3% significantly decreased the pitting potential value from 0.431 V at 4% NaCl to 0.364 V (2.74×10^4 A) at 6% NaCl as a result of early collapse of the passive film on GX4Cr. It also shows 3% NaCl is the threshold NaCl concentration for effective pitting resistance of GX4Cr. Excess Cl^- ions absorbed at the film solution interfaced overwhelmed the oxy-hydroxide layer consisting of Cr_2O_3 by substitution of O_2 atoms with Cl which continued to oxidize the steel at localized spots where the film breakage occurred. The passivation range values indicate the strength and resilience of the passive film on stainless steels. Addition of Cl^- ions significantly decreased the passivation range values of GX4Cr especially beyond 3% NaCl. This confirms application of GX4Cr is limited in industrial environments loaded with corrosive anions. Metastable pits are transient corrosion pits which forms following anodic polarization. The metastable pitting values show the transient pitting capacity of the steel and its tendency to quickly passivate. Most steels do not passivate after anodic polarization while some do passivate after extended metastable pitting activity which invariably shortens the passivation range of steels. At 0% NaCl, the metastable pitting value of GX4Cr is −0.209 V (3.11×10^5 A); this value increased to −0.277 V at 1% NaCl before progressively decreasing to −0.101 V. The decrease is due to prolonged anodic polarization and adsorption of excess Cl^- ions with increase in NaCl concentration which invariably increases the extent of oxidation reactions. The consequential effect of this observation is that the passivation range values of the steel decreases and hence the passive film weakens. 316Ti and 444St completely lost their passivation properties after 1% and 2% NaCl concentration as shown in Figs. 4(a), (b) and 5(a), (b). At 0% and 1% NaCl concentration, the pitting potential of 316Ti increased from 0.941 V to 0.950 V while the passivation range value increased from 1.019 V and 1.069 V indicating increased

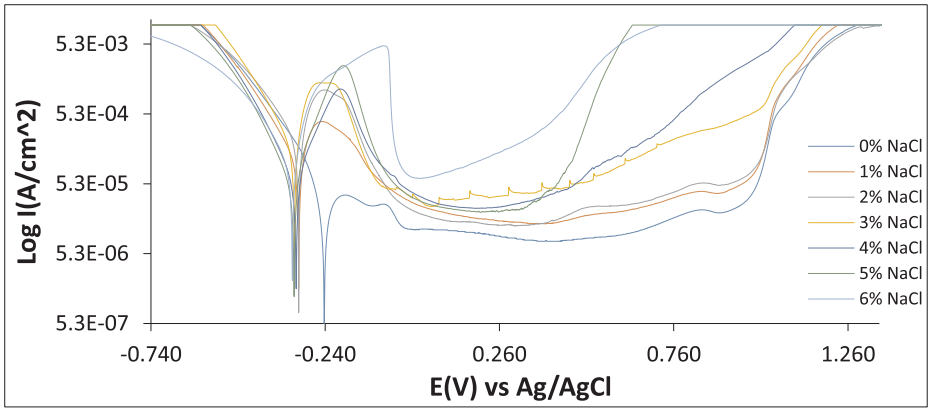

Fig. 2. Potentiodynamic polarization plots GX4Cr corrosion in 1 M H_2SO_4 solution at 0% − 6% NaCl concentration.

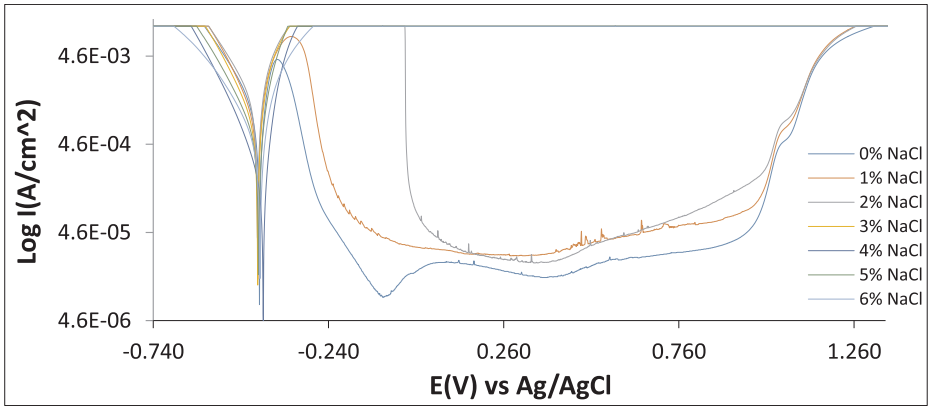

Fig. 3. Potentiodynamic polarization plots 444St corrosion in 1 M H_2SO_4 solution at 0% − 6% NaCl concentration.

localized corrosion resistance. However, the passivation properties of the steel disappeared after 1% due to complete breakdown of the passive film. Further analysis from optical microscopy shows no evidence of corrosion pits on the steel. The steel acidified in the corrosive media but was not prone to localized corrosion damage. The passivation of 444St at 2% NaCl occurred after prolonged anodic polarization which weakened the ability of the steel to passivate, though the steel eventually passivated at 0.002 V and broke down at 0.970 V corresponding to high pitting current of 1.74×10^4 A (0.970 V). This eventually results in relatively short passivation range (0.966 V). Beyond 2%, the passivation behaviour of 444St was completely absent despite the observation that the minimum passivation 444St passivation range of 0.970 V is much higher than the passivation range values obtained for GX4Cr at 1%–6% NaCl concentration. This suggests that the mechanism and composition of GX4Cr passive film is significantly different from 444St and possibly 316Ti. The reason for this lies with the elemental composition of the steels and their metallurgical properties.

Open circuit potential measurement

The open circuit corrosion potential (OCP) plots for 316Ti, GX4Cr and 444St corrosion at 0%, 1% and 6% NaCl concentration in 1 M H_2SO_4 solution are shown from Fig. 7(a) to (c). Fig. 7(a) shows the plots at 0% NaCl, Fig. 7(b) at 1% NaCl and Fig. 7(c) at 6% NaCl concentration respectively. The plots show GX4Cr is significantly more electropositive; hence more corrosion resistant than 316Ti and 444St stainless steels. This is due to formation and growth of resilient Cr_2O_3 protective film on GX4Cr. However, the electropositive values decrease with addition of Cl^- ions into the acid solution (1% and 6% NaCl concentration). At 0% NaCl, the OCP plot of GX4Cr initiated at

Table 2
Potentiodynamic polarization data for 316Ti, GX4Cr and 444St corrosion in 1 M H_2SO_4 solution at 0% − 6% NaCl concentration.

Sample	NaCl Conc. (%)	316Ti Corrosion Rate (mm/y)	Corrosion Current Density (A/cm^2)	Corrosion Potential (V)	Polarization Resistance, R_p (Ω)	Cathodic Potential, B_c (V/dec)	Anodic Potential, B_a (V/dec)
316Ti							
A	0	8.022	7.60E − 04	−0.419	17.44	−8.827	6.754
B	1	11.653	1.10E − 03	−0.406	23.27	−7.877	5.981
C	2	13.373	1.27E − 03	−0.402	20.28	−7.817	6.955
D	3	11.716	1.11E − 03	−0.401	23.14	−8.016	9.344
E	4	13.036	1.24E − 03	−0.400	20.21	−8.092	8.140
F	5	15.864	1.50E − 03	−0.403	17.10	−7.723	5.624
G	6	16.033	1.52E − 03	−0.404	16.86	−7.791	8.940
Sample	NaCl Conc. (%)	GX4Cr Corrosion Rate (mm/y)	Corrosion Current Density (A/cm^2)	Corrosion Potential (V)	Polarization Resistance, R_p (Ω)	Cathodic Potential, B_c (V/dec)	Anodic Potential, B_a (V/dec)
GX4Cr							
A	0	0.373	3.48E − 05	−0.243	739.20	−8.337	−1.841
B	1	2.124	1.98E − 04	−0.316	129.90	−8.272	−1.390
C	2	4.328	4.03E − 04	−0.316	63.79	−7.202	−0.168
D	3	4.073	3.79E − 04	−0.328	67.77	−8.756	0.167
E	4	1.165	1.08E − 04	−0.323	237.10	−9.961	11.050
F	5	1.056	9.83E − 05	−0.329	258.90	−10.39	13.050
G	6	1.066	9.92E − 05	−0.334	271.20	−8.191	6.591
Sample	NaCl Conc. (%)	444St Corrosion Rate (mm/y)	Corrosion Current Density (A/cm^2)	Corrosion Potential (V)	Polarization Resistance, R_p (Ω)	Cathodic Potential, B_c (V/dec)	Anodic Potential, B_a (V/dec)
444St							
A	0	15.945	1.48E − 03	−0.437	17.31	−6.739	9.617
B	1	18.373	1.71E − 03	−0.442	15.02	−7.937	4.188
C	2	20.844	1.94E − 03	−0.443	13.04	−5.427	6.273
D	3	14.924	1.39E − 03	−0.442	18.50	−8.033	7.144
E	4	11.185	1.04E − 03	−0.426	22.58	−9.459	10.600
F	5	10.714	9.97E − 04	−0.440	25.77	−7.749	9.280
G	6	7.784	7.25E − 04	−0.436	35.46	−6.986	7.315

Table 3
Potentiostatic data for 316Ti, GX4Cr and 444ST corrosion in 1 M H_2SO_4 solution at 0% − 6% NaCl concentration.

NaCl Conc. (%)	Metastable Pitting Potential (V)	Metastable Pitting Current (A)	Passivation Potential (V)	Passivation Current (A)	Pitting Potential (V)	Pitting Current (A)	Passivation Range (V)
316Ti							
0	−0.387	3.06E−03	−0.078	4.59E−05	0.941	4.08E−05	1.019
1	−0.336	6.06E−03	−0.119	2.51E−04	0.950	8.49E−05	1.069
NaCl Conc. (%)	Metastable Pitting Potential (V)	Metastable Pitting Current (A)	Passivation Potential (V)	Passivation Current (A)	Pitting Potential (V)	Pitting Current (A)	Passivation Range (V)
GX4Cr							
0	−0.209	3.11E−05	−0.162	3.42E−05	0.914	2.13E−05	1.076
1	−0.277	3.21E−04	−0.020	3.45E−05	0.920	4.35E−05	0.940
2	−0.272	8.80E−04	−0.011	2.20E−05	0.936	5.66E−05	0.947
3	−0.250	1.48E−03	−0.095	6.11E−05	0.981	5.29E−04	1.076
4	−0.201	1.19E−03	0.047	3.24E−05	0.431	4.07E−05	0.384
5	−0.198	2.46E−03	−0.013	4.01E−05	0.382	3.50E−05	0.395
6	−0.101	4.47E−03	−0.011	7.77E−05	0.364	2.74E−04	0.375
NaCl Conc. (%)	Metastable Pitting Potential (V)	Metastable Pitting Current (A)	Passivation Potential (V)	Passivation Current (A)	Pitting Potential (V)	Pitting Current (A)	Passivation Range (V)
444St							
0	−0.401	1.27E−03	−0.123	1.05E−05	0.913	3.62E−05	1.036
1	−0.373	6.38E−03	−0.092	4.16E−05	0.940	7.76E−05	1.032
2	−0.059	9.94E−03	0.004	9.11E−05	0.970	1.74E−04	0.966

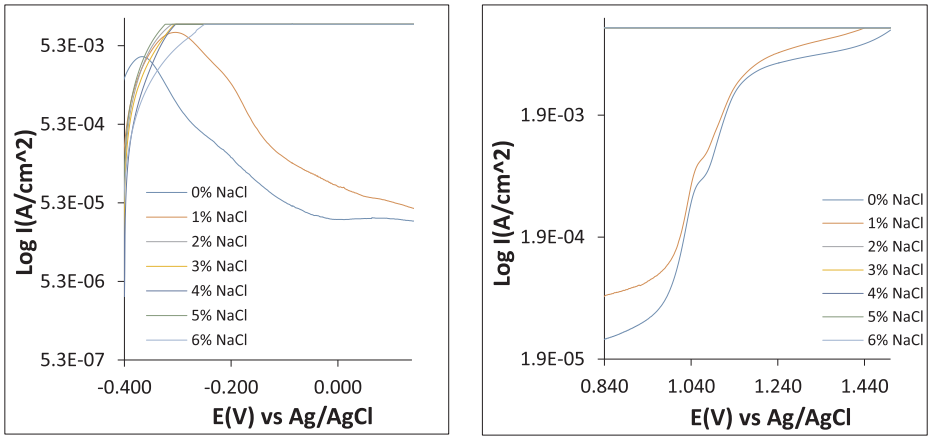

Fig. 4. Polarization plots of (a) metastable pitting portion and (b) stable pitting portion for 316Ti.

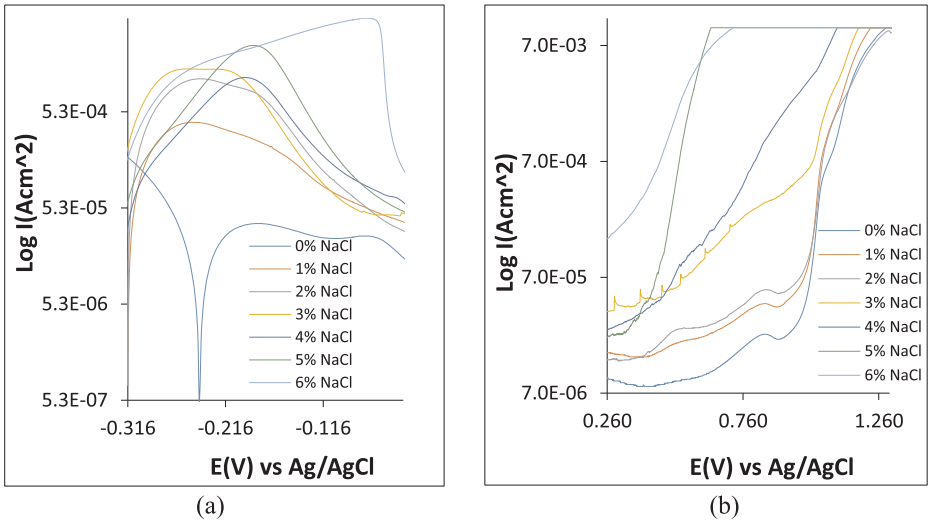

Fig. 5. Polarization plots of (a) metastable pitting portion and (b) stable pitting portion for GX4Cr.

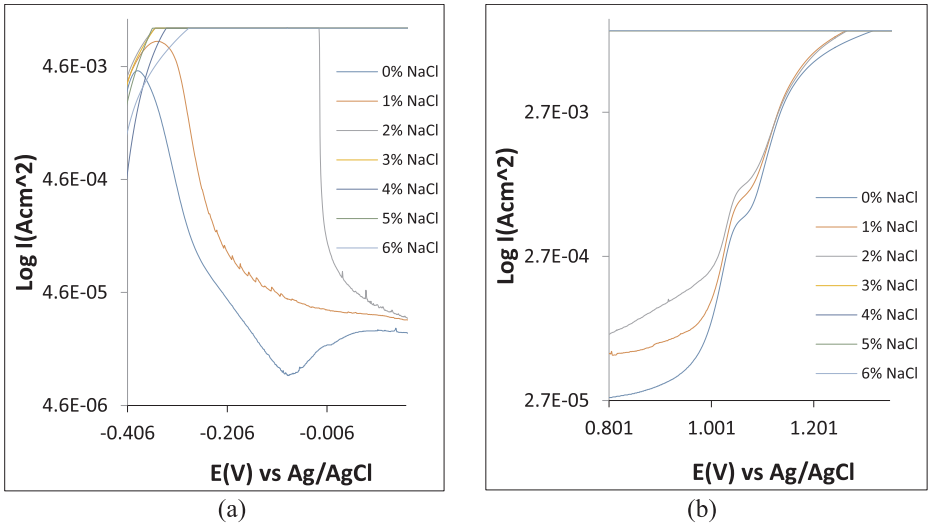

Fig. 6. Polarization plots of (a) metastable pitting portion and (b) stable pitting portion for 444St.

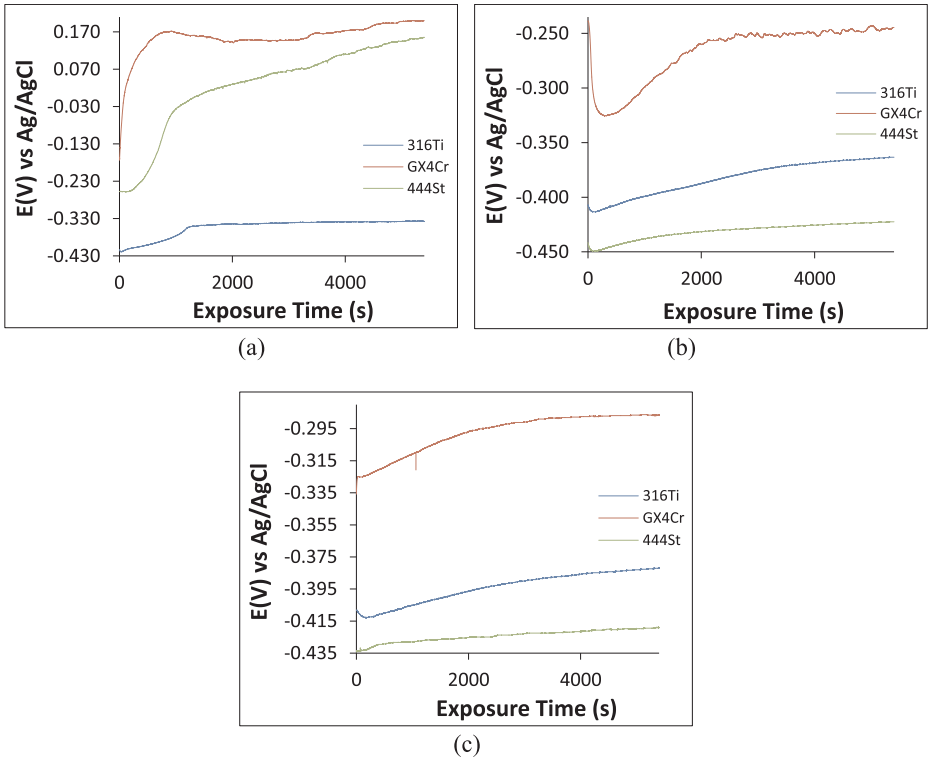

Fig. 7. Variation of open circuit corrosion potential versus exposure time for 316Ti, GX4Cr and 444St in 1 M H_2SO_4 solution at (a) 0% NaCl, (b) 1% NaCl and (c) 6% NaCl concentration.

−0.174 V (0 s) and displaced sharply (positively) to 0.153 V at 600 s due to instantaneous adsorption and chemical combination of with O_2 with Cr atoms to form the protective passive film on the steel. Further exposure till 5400 s had limited influence on the thermodynamic properties of the steel, but the subsequent OCP values show GX4Cr remained passive and resistant to corrosion throughout the exposure period. Increase in NaCl concentration decreased the electropositive values of OCP to values around −0.250 V at 1% NaCl [Fig. 7(b)] and −0.285 V at 6% NaCl [Fig. 7(c)]. The plot at 6% NaCl achieved relative stability at 3139.6 s (−0.290 V); however, at 1% NaCl the OCP plots was thermodynamically unstable from 1600 s (−0.274 V) to 5400 s (−0.245 V). This is due to active-passive transition of the plots resulting from the transient collapse and repassivation of the protective film as a result of Cl^- ion ingress. In the absence of Cl^- ion (0% NaCl), the OCP plot of 444St was significantly electropositive after 131.5 s due to oxide formation similar to GX4Cr steel up till 5400 s at which the potential is 0.200 V (value for excellent corrosion resistance). At 1% and 6% NaCl, the steel demonstrated weak resistance to the electrochemical actions of chlorides in the sulphate solution with highest OCP value of −0.422 V and −0.419 V at 5400 s. These values are associated with active corrosion reactions occurring on the steel. The variation of corrosion potential with exposure for 316Ti at 0%, 1% and 6% NaCl showed the steel is prone to active corrosion reactions at optimal electronegative potentials of −0.338 V, −0.363 V, −0.382 V (5400 s) compared to values obtained for GX4Cr steel. Its corrosion resistance without applied potentials is slightly higher than 444St at 1% and 6%

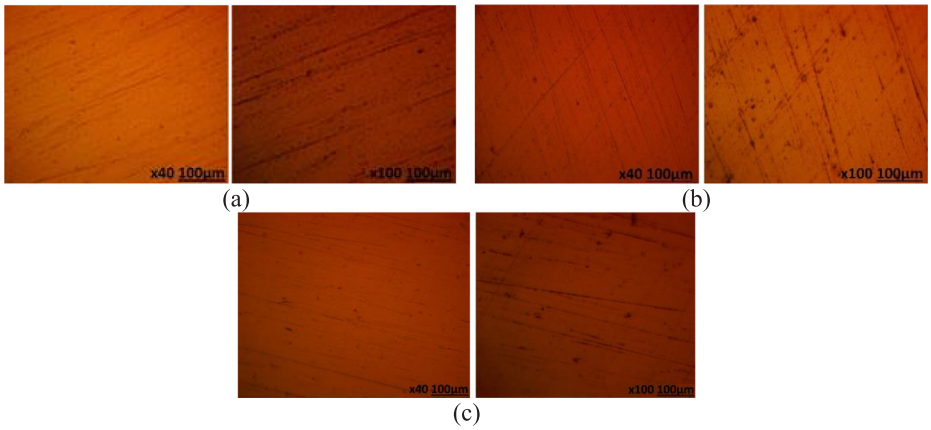

Fig. 8. Optical images of (a) 316Ti, (b) GX4Cr and (c) 444St before corrosion test.

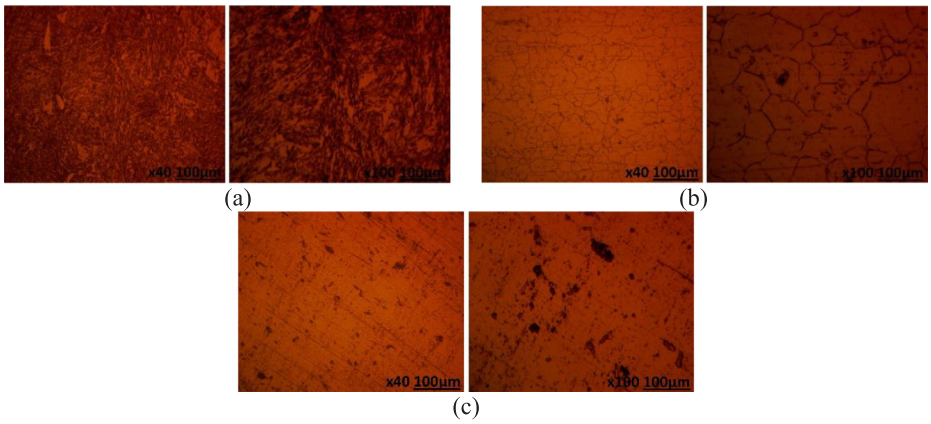

Fig. 9. Optical images of (a) 316Ti, (b) GX4Cr and (c) 444St after corrosion from 1 M H_2SO_4/0% NaCl concentration.

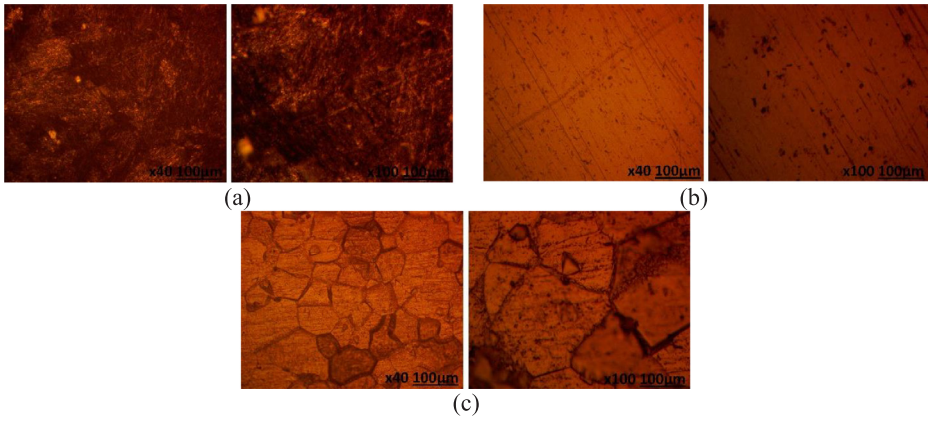

Fig. 10. Optical images of (a) 316Ti, (b) GX4Cr and (c) 444St after corrosion from 1 M H_2SO_4/1% NaCl concentration.

NaCl.

Optical microscopy studies

Optical images (mag. ×40 and ×100) of 316Ti, GX4Cr and 444St morphology before corrosion, and after corrosion from 1 M H_2SO_4 solution at 0%, 1% and 6% NaCl concentration are shown from Figs. 8(a) to 11(c). At 0% NaCl, the morphology of 316Ti [Fig. 9(a)] showed severe general deterioration. However, corrosion pits were absent. It is probable that the presence of Ti in 316 steel is responsible for this phenomenon as it was meant to reduce the formation of intercrystalline corrosion. The morphology of GX4Cr [Fig. 9(b)] exhibited intergranular corrosion, though corrosion pits do form which appears to be superficial and shallow. The relatively low corrosion rates of GX4Cr suggest the corrosion along the grain boundary could be mere etching of the steel surface which later stifled out as a result of substantial amount of Mo within the steel microstructure. Fig. 9(c) shows the morphology of 444St with numerous corrosion pits signifying relatively weak resistance to pitting corrosion. At 1% NaCl, the morphology of GX4Cr [Fig. 10(b)] had deteriorated further with numerous corrosion pits; at this concentration the extent of surface deterioration is quite similar to that of 444St [Fig. 10(c)]. No visible change occurred in the morphology of 316Ti [Fig. 10(a)] compared to Fig. 9(a)]. The extent of morphological deterioration on GX4Cr [Fig. 11(b)] decreased at 6%

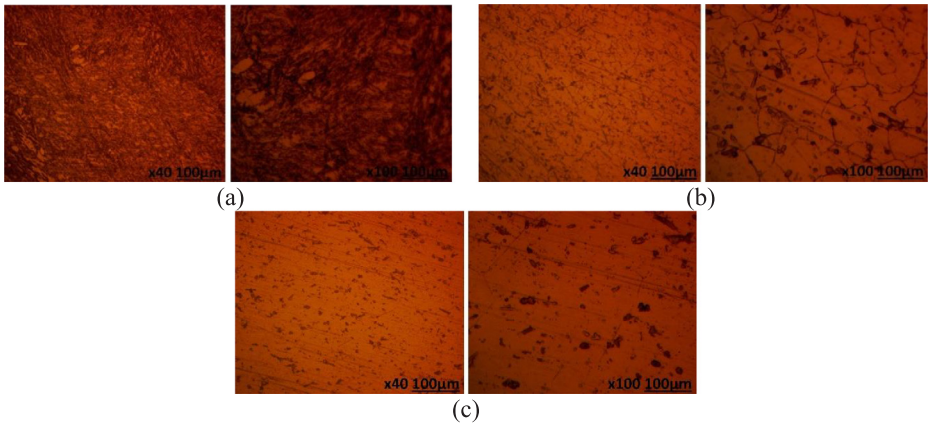

Fig. 11. Optical images of (a) 316Ti, (b) GX4Cr and (c) 444St after corrosion from 1 M H_2SO_4/6% NaCl concentration.

NaCl, probably due to inhibiting action of SO_4^{2-} ions in the presence of excess Cl^- ions. There is also the possibility of competitive adsorption between both ions which has less detrimental effect on the steel surface. At this concentration the morphology of 444ST [Fig. 11(c)] also improved with no visible corrosion pits. However, carbide precipitation occurred on 316Ti resulting in a darkened morphology as shown in Fig. 11(a)

Conclusion

Comparative assessment of the corrosion resistance and passivation characteristics of 316Ti austenitic, GX4CrNiMo16-5-1 martensitic and 444 ferritic stainless steels in acid chloride solution showed GX4CrNiMo16-5-1 steel exhibited the highest general and localized corrosion resistance. Its passive film remained resilient though weakened at all chloride concentrations studied compared to 316Ti and 444 steels whose passivity collapsed at low chloride concentration. The continuous electropositive displacement of GX4CrNiMo16-5-1 OCP plot confirmed the continuous growth of its protective oxide film compared to 316Ti and 444 steels whose OCP plot were comparatively electronegative signifying active corrosion reaction mechanisms.

Acknowledgement

The author appreciates Covenant University for their support, research funding and provision of research facilities.

Appendix A. Supplementary data

Supplementary data to this article can be found online at https://doi.org/10.1016/j.rinp.2019.102423.

References

[1] Black J. Biological performance of materials: Fundamentals of Biocompatibility. 4th ed. Boca Raton: CRC Press; 2006.
[2] Číhal V. Stainless steels and alloys. (in Czech). Praha: Academia; 1999.
[3] Incoloy Alloy 800H & 800HT, Technical Bulletin, Special Metals Publication SMC-047. http://www.specialmetals.com [Retrieved 1st April, 2019].
[4] Liptáková T. Pitting corrosion of stainless steels. Mater Eng 2011;18:115–20.
[5] Szklarska Salowska Z. Pitting and crevice corrosion. Houston Texas: NACE International; 2005.
[6] Rodabaugh RD. Surface cleaning. ASM Handbook. 3rd ed. USA: ASM International; 1999.
[7] Feng H, Li H, Wu X, Jiang Z, Zhao Si, Zhang T, et al. Effect of nitrogen on corrosion behaviour of a novel high nitrogen medium-entropy alloy CrCoNiN manufactured by pressurized metallurgy. J Mater Sci Technol 2018;34(10):1781–90.
[8] Burstein GT, Pistorious PC. Surface roughness and the metastable pitting of stainless steel in chloride solutions. Corrosion 1995;51(5):380–5.
[9] Zhang S, Li H, Jiang Z, Zhang B, Li Z, Wu J, et al. Effects of Cr and Mo on precipitation behavior and associated intergranular corrosion susceptibility of super-austenitic stainless steel S32654. Mater Charact 2019;152:141–50.
[10] Burkert A, Lehmann J, Burkert A, Mietz J, Gumpel P. Technical and economical stainless steel alternatives for civil engineering applications. Mater Corros 2013;64:1–17.
[11] Lee JB. Effects of alloying elements, Cr, Mo and N on repassivation characteristics of stainless steels using the abrading electrode technique. Mater Chem Phys 2006;99(2–3):224–34.
[12] Hong T, Nagumo M. The effect of chloride concentration on early stages of pitting for 304 stainless steel revealed by the AC impedance method. Corros Sci 1997;39(2):285–93.
[13] Loto RT, Loto CA. Evaluation of the localized corrosion resistance of 316 L austenitic and 430Ti ferritic stainless steel in aqueous chloride/sulphate media for application in petrochemical crude distillation units. Mater Res Express 2019;6:086516https://doi.org/10.1088/2053-1591/ab1a11.
[14] Loto RT. Potentiodynamic polarization studies of the pitting corrosion resistance and passivation behavior of P4 low carbon mold steel in chloride and acid chloride solution. Mater Res Express 2018;5:116509https://doi.org/10.1088/2053-1591/aadc84.
[15] Loto RT. Effect of elevated temperature on the corrosion polarization of NO7718 and NO7208 nickel alloys in hot acid chloride solution. J Bio Tribo Corros 2018;4:71. https://doi.org/10.1007/s40735-018-0190-8.
[16] Loto RT, Loto CA. Potentiodynamic polarization behavior and pitting corrosion analysis of 2101 duplex and 301 austenitic stainless steel in sulfuric acid concentrations. J Fail Anal Prev 2017;17(4):672–9. https://doi.org/10.1007/s11668-017-0291-6.
[17] Loto RT. Study of the corrosion resistance of type 304L and 316 austenitic stainless steels in acid chloride solution. Orient J Chem 2017;33(3):1090–6. https://doi.org/10.13005/ojc/330304.
[18] Loto RT. Electrochemical corrosion characteristics of 439 ferritic, 301 austenitic, S32101 duplex and 420 martensitic stainless steel in sulfuric acid/NaCl solution. J Bio Tribo Corros 2017;3(24). https://doi.org/10.1007/s40735-017-0084-1.
[19] Dai N, Zhang L-C, Zhang J, Chen Q, Wu M. Corrosion behavior of selective laser melted Ti-6Al-4 V alloy in NaCl solution. Corros Sci 2016;102:484–9.
[20] Bautist A, Blanco G, Velasco F. Corrosion behaviour of low-nickel austenitic stainless steels reinforcements: a comparative study in simulated pore solutions. Cem Concr Res 2006;36(10):1922–30. https://doi.org/10.1016/j.cemconres.2005.10.009.
[21] Zatkalíková V, Bukovina M, Škorík V, Lenka Petreková L. Pitting corrosion of AISI 316Ti stainless steel with polished surface. Mat Eng 2010;17(2):15–9.
[22] Marques RA, Rogero SO, Terada M, Pieretti EF, Costa I. Localized corrosion resistance and cytotoxicity evaluation of ferritic stainless steels for use in implantable dental devices with magnetic connections. Int J Electrochem Sci 2014;9:1340–54.
[23] Bellezze T, Roventi G, Quaranta A, Fratesi R. Improvement of pitting corrosion resistance of AISI 444 stainless steel to make it a possible substitute for AISI 304L and 316L in hot natural waters. Mater Corros 2008;59(9):727–31.
[24] Park C-J, Lee Y-H. Initiation and repassivation of crevice corrosion of type 444 stainless steel in chloride solution. Metallurgical Mater Int 2004;10(5):447–51.
[25] Venkatesan P, Anand B, Matheswaran P. Influence of formazan derivatives on corrosion inhibition of mild steel in hydrochloric acid medium. E-J Chem 2009;6(S1):S438–44.
[26] Qin P, Chen Y, Liu Y-J, Zhang J, Chen L-Y, Li Y, et al. Resemblance in corrosion behavior of selective laser melted and traditional monolithic β Ti-24Nb-4Zr-8Sn alloy. ACS Biomater Sci Eng 2018;5(2):1141–9.
[27] Loto RT. Corrosion inhibition performance of the synergistic effect of rosmarinus officinalis and 5-bromovanillin on 1018 carbon steel in dilute acid media. J Fail Anal Prev 2017;17(5):1031–43.